Applied Catalysis B: Environmental 142–143 (2013) 72–79

Contents lists available at SciVerse ScienceDirect

Applied Catalysis B: Environmental

journal homepage: www.elsevier.com/locate/apcatb

Well-dispersed palladium supported on ordered mesoporous Co_3O_4 for catalytic oxidation of o-xylene☆

Yafei Wang, Changbin Zhang, Fudong Liu, Hong He*

Research Centre for Eco-Environmental Sciences, Chinese Academy of Sciences, Beijing 100085, PR China

ARTICLE INFO

Article history:
Received 1 March 2013
Received in revised form 3 May 2013
Accepted 5 May 2013
Available online 13 May 2013

Keywords:
Ordered mesoporous
Cobalt oxide
Palladium
Catalytic oxidation
o-Xylene

ABSTRACT

Ordered mesoporous Co_3O_4(3D) and Pd/Co_3O_4(3D) were prepared by a nanocasting route using mesoporous silica (KIT-6) as a hard template. In addition, Pd/Co_3O_4(3DL) was prepared as a reference by post-impregnation of Pd in Co_3O_4(3D). All catalysts were tested for the total oxidation of o-xylene in the temperature range of 150–300 °C. The mesoporous Co_3O_4(3D) showed better activity than bulk Co_3O_4 (B) for o-xylene oxidation. As for Pd-loaded samples, Pd/Co_3O_4(3D) had much higher activity than Pd/Co_3O_4(3DL). These catalysts were characterized by BET, XRD, TEM, XPS, H_2-TPR and XAFS methods. The characterization results show that the Pd/Co_3O_4(3D) synthesized by in situ nanocasting presented a more ordered mesostructure and more well-dispersed PdO species than the Pd/Co_3O_4(3DL) prepared with the post-impregnation method, which account for its excellent activity for o-xylene oxidation. In addition, it was demonstrated that Pd in the oxidized state is the active site for o-xylene oxidation.

1. Introduction

BTX (benzene, toluene, and xylene) are some of the major volatile organic compounds (VOCs), with high toxic potential to human health [1,2]. Catalytic oxidation is considered to be the most promising pathway for the removal of VOCs owing to its easy application, high efficiency and low cost [3,4]. Catalytic oxidation of VOCs over supported noble metals and metal oxides catalysts has been widely studied [4,5]. Pd-based catalysts are recognized as the most promising catalysts for VOC removal in the low temperature range, owing to their high catalytic activity and low price. As for BTX oxidation, Pd-based catalysts have also demonstrated superior performance compared to other noble metals [3,5,6].

Although Pd catalysts have been widely studied for catalytic oxidation of VOCs, there is no consensus concerning the behavior of Pd active species during the oxidation reaction. Several authors stated that the oxidized state of Pd is more important than metallic Pd for performance in VOC oxidation [3,7], whereas many researchers affirmed the opposite [6,8,9]. Another explanation involves both metallic and oxidized states [10]. The textural properties of the support have also been found to have an important influence on the catalytic performance of supported Pd catalysts. Okumura [11] suggested that the catalytic activity of Pd was related to the acid–base properties of supports such as Al_2O_3, MgO, SiO_2, SnO_2, Nb_2O_5, ZrO_2 and WO_3, and that metallic Pd stabilized by weak acid supports was responsible for the high activity in VOC oxidation. For zeolite supports, the activity for the total oxidation of BTX was found to depend on the type of zeolite and cation in the zeolite, which affected the Pd dispersion and PdO reducibility [12]. Porous silica supports also promote the activity of Pd catalysts because of the stabilization of active Pd species in the porous structure [13].

Recently, mesoporous cobalt oxides, with the nature of transition metal oxides and porosity characteristics of porous materials, have attracted great interest due to their many potential applications in catalysis and as catalyst supports [14–16]. The material can be prepared using a hard template, which provides stable support for the synthesis of highly ordered crystalline mesoporous materials during high-temperature crystallization [14–19]. The three-dimensional ordered mesoporous cobalt oxide has been shown to be an effective catalyst and catalyst support because it can facilitate the absorption and diffusion of reactant molecules in its open porous system [19–21].

In this work, we prepared mesoporous Pd/Co_3O_4 catalysts using in situ nanocasting and post-impregnation, respectively, and tested their activities for the low temperature catalytic oxidation of o-xylene. Catalysts were then characterized by BET, XRD, TEM, XPS, H_2-TPR and XAFS methods. The effects of preparation methods on the textural and chemical properties of Pd/Co_3O_4, such as the mesoporous structure, Pd species dispersion, oxidation-reduction

* Corresponding author. Tel.: +86 10 6284 9123; fax: +86 10 6284 9123.
E-mail address: honghe@rcees.ac.cn (H. He).
URL: http://hehong.rcees.ac.cn (H. He).

0926-3373/$ – see front matter © 2013 Elsevier B.V. All rights reserved.
http://dx.doi.org/10.1016/j.apcatb.2013.05.003

properties, were discussed and subsequently correlated with their activities.

2. Experimental

2.1. Catalyst preparation

Mesoporous Co_3O_4(3D) and 1 wt% Pd/Co_3O_4(3D) were prepared using 3D cubic KIT-6 [22] as a hard template. Typically, an ethanol solution of 11 mL 0.8 M $Co(NO_3)_2$ was placed in a glass cup and stirred at room temperature for 5 min. Afterwards, 0.5 g KIT-6 was added and stirred for 2 h. The ethanol was removed by evaporation through heating the mixture overnight at 40 °C. Then, the resulting powder was heated in a glass bottle (12 cm × 4 cm) with a cover in an oven at 300 °C for 3 h to completely decompose the nitrate species. Finally, the silica template was removed by 2 M NaOH at room temperature. The material was recovered by centrifugation, washed with water and dried at 60 °C. The obtained black powder was Co_3O_4(3D). 1 wt% Pd/Co_3O_4(3D) was prepared by the same procedure with a mixed solution of 11 mL 0.8 M $Co(NO_3)_2$ and 4.5 mL 0.0018 g mL^{-1} $Pd(NO_3)_2$ solution. 1 wt% Pd/Co_3O_4(3DL) was prepared by post-impregnation using Co_3O_4(3D) with an aqueous solution of $Pd(NO_3)_2$. Bulk Co_3O_4(B) was prepared by precipitation [23] and the bulk Pd/Co_3O_4(BL) was prepared by post-impregnation using Co_3O_4(B) with an aqueous solution of $Pd(NO_3)_2$.

2.2. Catalyst characterization

Powder X-ray diffraction (XRD) was used to identify the crystalline phases present in the catalysts. A Bruker D8 Advance diffractometer with a monochromatic Cu Kα source operated at 40 kV and 40 mA was used. TEM images were obtained using a JEOL JEM-2100 microscope, operating at 200 kV. N_2 adsorption–desorption isotherms were measured using a Quantachrome Quadrasorb IQ at liquid nitrogen temperature (77 K). X-ray photoemission (XPS) measurements were recorded on a Scanning X-ray Microprobe (AXIS Ultra, Kratos Analytical, Inc.). Binding energy was calibrated with C1s = 284.8 eV.

The H_2 temperature programmed reduction (H_2-TPR) tests were carried out with a mass spectrometer (Hiden HPR20). Prior to each TPR run, the catalyst was pretreated in an air flow at 300 °C in a quartz reactor. After cooling the reactor to room temperature, Ar gas was fed into the reactor at 30 mL min^{-1} for 30 min to purge any residual oxygen. The catalyst was then heated to 700 °C at a constant heating rate of 10 °C min^{-1} under 5% H_2–Ar flow of 30 mL min^{-1}.

The XANES and EXAFS of Pd–K and Co–K edges in a series of Pd- and Co-containing samples and reference samples were measured in florescence mode and transmission mode, respectively, at room temperature on the BL14W1 beam line, Shanghai Synchrotron Radiation Facility (SSRF). The storage ring was operated at 3.5 GeV with 200 mA as an average storage current. The synchrotron radiation was monochromatized with a Si (3 1 1) double crystal monochromator. Data were analyzed using Athena and Artemis from the Ifeffit 1.2.11 software package [24]. XANES spectra were normalized with the edge height. The EXAFS oscillation $\chi(k)$ was extracted using spline smoothing with the Cook–Sayers criterion [25] and the filtered k^3-weighted $\chi(k)$ was Fourier transformed into R space in the k ranges of 2.5–12.0 Å^{-1} for Pd–K and 2.5–13.0 Å^{-1} for Co–K with a Hanning function window. In the curve-fitting step, the possible backscattering amplitude and phase shift were calculated using FEFF8.4 code [26].

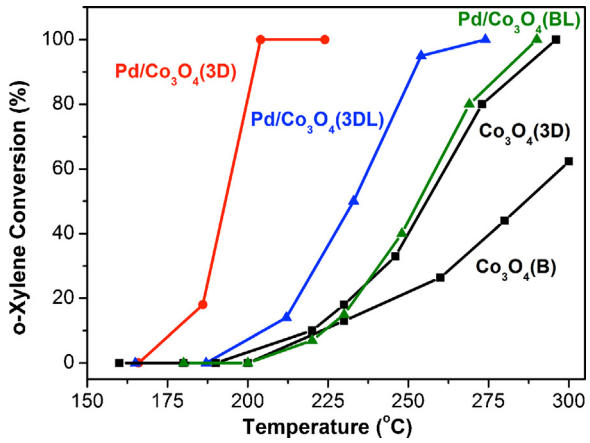

Fig. 1. o-Xylene conversion as a function of reaction temperature over the catalysts under the condition of o-xylene concentration = 150 ppm in air, the total flow is 100 mL min^{-1}.

2.3. Catalytic activity tests

The catalytic activities of the catalysts were evaluated in a continuous flow fixed-bed quartz microreactor between 150 and 300 °C with 100 mg of catalyst (40–60 mesh). The reactant feed (flow rate = 100 mL min^{-1}) was composed of 150 ppm o-xylene and air, with the weight hourly space velocity (WHSV) of 60,000 mL g^{-1} h^{-1}. In order to measure the specific activity of Pd/Co_3O_4(3D) at 230 °C, the Pd/Co_3O_4(3D) was also tested in a total flow rate of 400 mL min^{-1} (WHSV: 240,000 mL g^{-1} h^{-1}) to keep the o-xylene conversion below 100%. In addition, stability tests of Pd/Co_3O_4(3D) in the presence of 1% H_2O or 1000 ppm CO_2 were also performed at 230 °C with a total flow rate of 400 mL min^{-1}. The outlet gas was analyzed online by a GC-MS (Agilent 6890-5973N, HP 5MS) and a GC equipped with FID detector (Shangfen GC-112A, TDX-01 column).

3. Results and discussion

3.1. Catalytic activity

The catalytic performance of the samples for the oxidation of o-xylene at a WHSV of 60,000 mL g^{-1} h^{-1} are shown in Fig. 1. In all tests, CO_2 and H_2O were found to be the only products and the CO_2 selectivity was around 99.5%, indicating that o-xylene can be completely oxidized over these materials. The mesoporous samples showed higher activity than the bulk ones due to the fact that the mesostructure is favorable for the adsorption and diffusion of VOC molecules [19,20]. It is also clear that the Pd-based catalysts (Pd/Co_3O_4(3D), Pd/Co_3O_4(3DL) and Pd/Co_3O_4(BL)) showed much better activity than the neat Co_3O_4(3D) or Co_3O_4(B). The Pd/Co_3O_4(3D) showed the highest activity and the Pd/Co_3O_4(BL) exhibited the lowest catalytic activity among the Pd-based catalysts. The reaction temperatures $T_{50\%}$ and $T_{90\%}$ (corresponding to VOC conversion = 50% and 90%) were used to evaluate the catalytic performance and are summarized in Table 1. It is seen that a $T_{90\%}$ value of 196 °C for o-xylene oxidation was achieved over Pd/Co_3O_4(3D), whereas the $T_{90\%}$ value was 254 °C for o-xylene oxidation over the Pd/Co_3O_4(3DL) catalysts.

The catalytic performance of Pd/Co_3O_4(3D) for o-xylene oxidation was stable after 2 runs (Fig. S1). In addition, the catalytic stability of Pd/Co_3O_4(3D) in the presence of CO_2 and H_2O was investigated. The results (Fig. S2) showed that the addition of 1% H_2O and 1000 ppm CO_2 to the feeding gas had no obvious effect on the o-xylene conversion, further indicating that the

Table 1
Conversions ($T_{90\%}$, $T_{50\%}$ and X_{230}) of the o-xylene over the catalysts.

Catalyst	$T_{50\%}$ (°C)	$T_{90\%}$ (°C)	X_{230} (%)
Co_3O_4(B)	291	–	13
Co_3O_4(3D)	256	285	18
Pd/Co_3O_4(BL)	253	279	15
Pd/Co_3O_4(3D)	193	204	90[a]
Pd/Co_3O_4(3DL)	232	254	50

Reaction condition: o-xylene concentration = 150 ppm in air, total flow 100 mL min^{-1}.
[a] Unlike the other catalysts, the total flow for Pd/Co_3O_4(3D) was increased to 400 mL min^{-1}.

Pd/Co_3O_4(3D) had high stability and high resistance to CO_2 and H_2O.

3.2. Catalyst characterization

3.2.1. XRD

The low-angle XRD patterns of the Pd/Co_3O_4(3DL) and Pd/Co_3O_4(3D) samples are shown in Fig. 2. The low-angle XRD peaks indicate that the mesostructures of the metal oxides were similar to that of the template. For Co_3O_4(3D), its pattern shows (2 1 1), (2 2 0) and (3 3 2) well-resolved XRD peaks in the region of 2θ = 0.8–2.8°, which could be assigned to the planes of a 3D cubic structure, indicating that the ordered mesoporous structure was completely replaced by cobalt oxide. The reflections (2 1 1) and (2 2 0) observed for Pd/Co_3O_4(3D) mean that the mesostructure still remained in this sample. Therefore, Pd addition did not significantly affect the formation of the mesoporous structure of Co_3O_4(3D). In contrast, the Pd/Co_3O_4(3DL) samples only presented the (2 1 1) reflection at 2θ value of around 1° with a weak peak intensity lower than that in the Co_3O_4(3D) and Pd/Co_3O_4(3D) samples, suggesting that the mesostructure in Pd/Co_3O_4(3DL) was less ordered than that in Pd/Co_3O_4(3D).

From the large-angle XRD in Fig. 3, it can be seen that these materials exhibited 31.3°, 36.9°, 38.2°, 44.5°, 55.6°, 59.4°, and 65.3° (2θ) peaks, which are attributable to the cobalt oxide Co_3O_4 according to JCPDS PDF 74-1657. The nanoparticle sizes of mesoporous cobalt oxide were all about 14–16 nm as calculated from the XRD peaks. No characteristic diffraction peak of Pd or PdO can be observed in Fig. 3, suggesting that PdO was well dispersed on Co_3O_4(3D) for both Pd/Co_3O_4(3D) and Pd/Co_3O_4(3DL).

3.2.2. BET

The N_2 adsorption–desorption isotherms and pore size distributions (inset) of the catalysts are presented in Fig. 4. Slightly distorted type-IV isotherms in the relative pressure range of 0.4–0.8 of the sorption curves of Co_3O_4(3D) confirmed the formation of a mesopore structure [27]. From the pore size distribution data (inset in Fig. 4), Co_3O_4(3D) was found to have a uniform pore size distribution with a primary mesopore diameter of 3.8 nm Pd/Co_3O_4(3D) showed isotherms and pore size distribution similar to Co_3O_4(3D). Pd/Co_3O_4(3DL) also had type-IV isotherms but with smaller primary mesopore diameter (2.5 nm).

The textural properties of these samples are summarized in Table 2. The surface area and pore size distribution of Pd/Co_3O_4(3D) were similar to those of Co_3O_4(3D) (Fig. 4 and Table 2). In contrast, the surface area of Pd/Co_3O_4(3DL) decreased from 82 to 65 m^2 g^{-1} after Pd post-impregnation, and the pore diameter and the pore volume also decreased, which means that the mesostructure of the support was partially destroyed by post-impregnation. The specific activities of all samples at 230 °C were calculated based on the BET surface areas (In order to measure the specific activity of Pd/Co_3O_4(3D) at 230 °C, total flow rate was increased to 400 mL min^{-1} to keep the o-xylene conversion below 100%.) and the o-xylene conversions at 230 °C (Table 1), and the calculated results are shown in Table 2. The Pd/Co_3O_4(3D) exhibited the highest specific activity, and the 3D mesoporous catalysts had higher

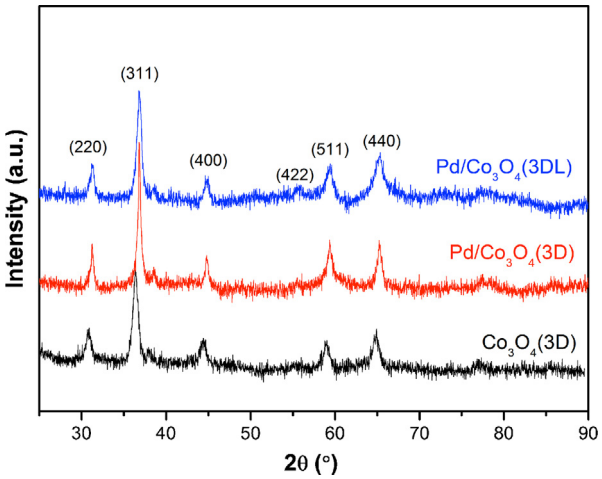

Fig. 3. The large angle XRD of the mesoporous catalysts.

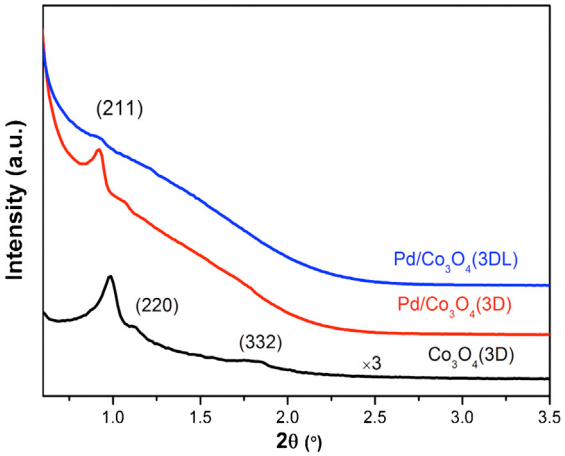

Fig. 2. Low angle XRD of the mesoporous catalysts.

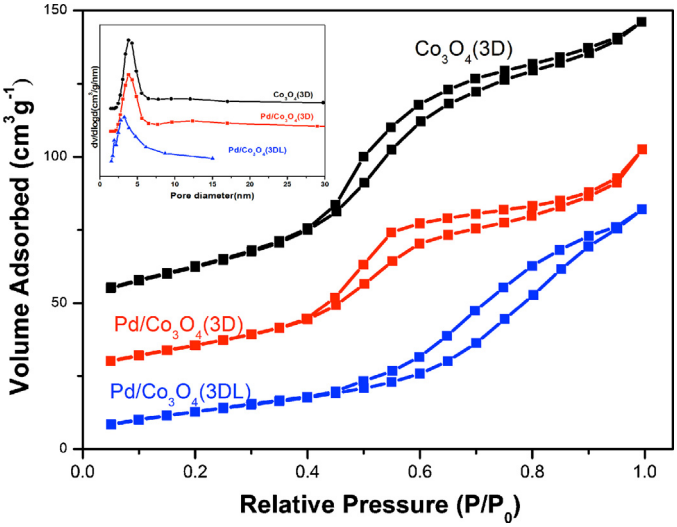

Fig. 4. N_2 adsorption–desorption isotherms and pore size distributions of the catalysts.

Table 2
Physical properties and specific activities (230 °C) of the catalysts.

Catalyst	Surface area ($m^2\ g^{-1}$)	Average pore diameter (nm)	Pore volume ($cm^3\ g^{-1}$)	Specific activity (10^{-7} mol s^{-1} $(m^2)^{-1}$)
Co_3O_4(B)	98	13	0.31	5.3
Co_3O_4(3D)	82	8.8	0.18	8.7
Pd/Co_3O_4(BL)	108	10	0.28	5.6
Pd/Co_3O_4(3D)	84	7.6	0.16	172
Pd/Co_3O_4(3DL)	65	6.3	0.13	30

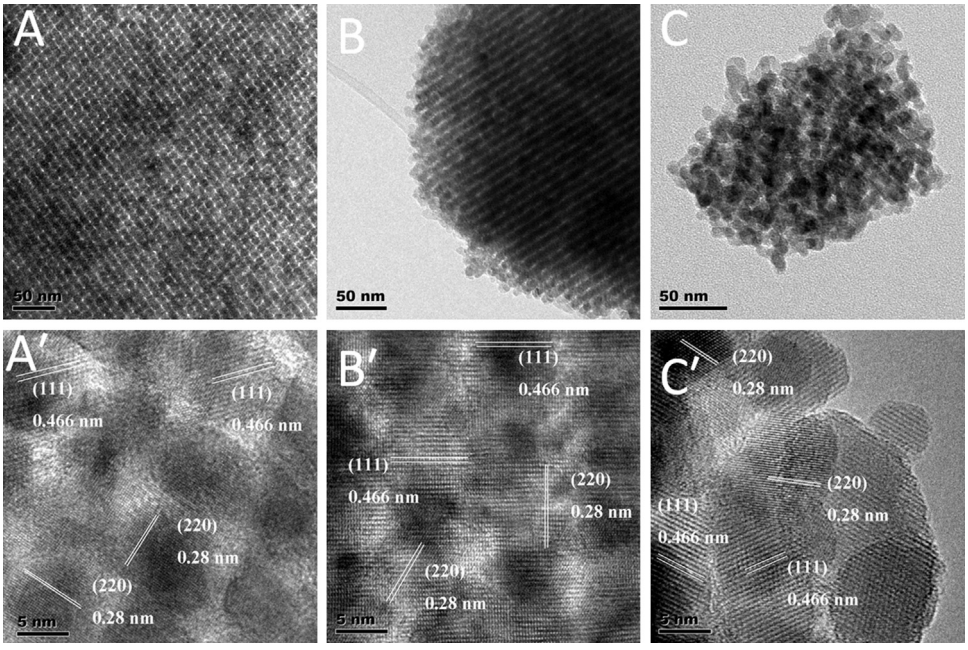

Fig. 5. TEM and HRTEM images of the catalysts: (A and A′) Co_3O_4(3D), (B and B′) Pd/Co_3O_4(3D) and (C and C′) Pd/Co_3O_4(3DL).

specific activity than the bulk catalysts, indicating that the o-xylene oxidation reaction is structure sensitive.

3.2.3. TEM and HR-TEM

As shown in Fig. 5A–C, an ordered mesoporous structure was clearly observed in Co_3O_4(3D), confirming that the template was replaced completely by Co_3O_4. Pd/Co_3O_4(3D) also showed a uniform mesostructure, but Pd/Co_3O_4(3DL) showed a less ordered mesostructure. As shown in Fig. 5A′–C′, HR-TEM images of the Co_3O_4 and Pd/Co_3O_4 samples show the 0.28 nm lattice spacing of Co_3O_4 (2 2 0) as well as the 0.46 nm (1 1 1) lattice spacing, and PdO was not observed by HRTEM. For Co_3O_4, the (1 1 1) planes are believed to be inactive crystal planes because they contain only Co^{2+} [28]. The (1 1 0) lattice planes, which are parallel to (2 2 0), consist solely of Co^{3+} cations [28], and provide favorable sites for o-xylene and oxygen adsorption as active sites for catalytic oxidation.

3.2.4. H_2-TPR

To investigate the reducibility of the samples, the H_2-TPR profiles of the catalysts were measured. As shown in Fig. 6, Co_3O_4(3D) shows two reduction peaks at 320 and 430 °C assigned to the $Co^{3+} \rightarrow Co^{2+}$ ($Peak_{II}$) and $Co^{2+} \rightarrow Co^{\circ}$ ($Peak_{III}$) reductions [21], respectively. After Pd was in situ loaded, both $Peak_{II}$ and $Peak_{III}$ were shifted to 276 and 390 °C, indicating that the introduction of PdO facilitated the reduction of Co_3O_4(3D) due to a H_2 spillover effect. In addition, a sharp reduction peak ($Peak_I$) at 174 °C due to PdO reduction was also observed for Pd/Co_3O_4(3D), showing that PdO was well dispersed on the Co_3O_4(3D) sample. The well-dispersed PdO nanoparticles interact strongly with the Co_3O_4(3D) support. This is confirmed by the reduction temperature of PdO in Pd/Co_3O_4(3D), which was higher than that (165 °C) of Pd/Co_3O_4(3DL). As for the Pd/Co_3O_4(3DL) sample, $Peak_{II}$ and $Peak_{III}$ shifted to 260 and 360 °C due to the promoting effect of PdO. A PdO reduction peak appeared at 165 °C for Pd/Co_3O_4(3DL), but the peak was much wider than that of Pd/Co_3O_4(3D).

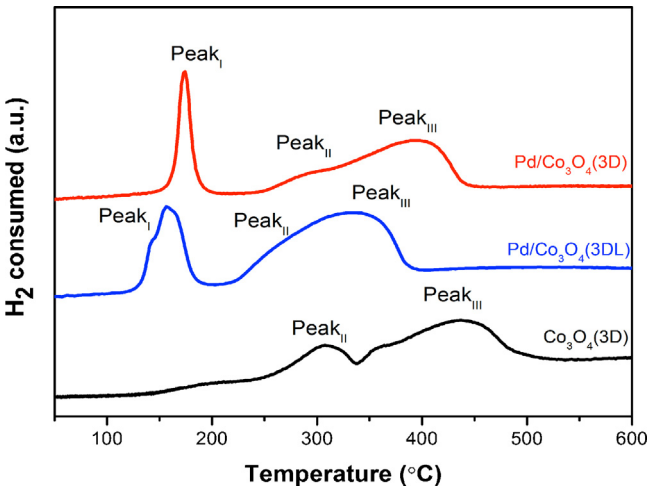

Fig. 6. H_2-TPR profiles of the catalysts.

Table 3
Curve fitting results of Pd K-edge EXAFS in Pd-containing samples and reference samples.

Sample	Shell	CN[a]	R[b] (Å)	σ^2 [c] (10^{-3} Å^2)	R factor (%)
Pd foil	Pd–Pd	12.0	2.74	6.7	2.5
PdO	Pd–O	3.6	2.02	3.7	9.2
	Pd–O–Pd	7.9	3.14	6.6	
Pd/Co_3O_4(3D)	Pd–O	3.4	2.02	12.1	6.6
	Pd–O–Pd	3.5	3.13	9.2	
Pd/Co_3O_4(3DL)	Pd–O	3.5	2.02	16.9	15.9
	Pd–O–Pd	4.6	3.15	10.4	
Pd/Co_3O_4(3DR)	Pd–Pd	6.6	2.72	12.1	14.7
Pd/Co_3O_4(3DLR)	Pd–Pd	8.8	2.75	16.1	6.9

[a] CN: coordination number.
[b] R: bond distance.
[c] σ: Debye–Waller factor.

3.2.5. XPS

The XPS analysis was performed to verify the state of Pd and Co on the surface. Fig. 7A shows the Pd 3d XPS spectra of Pd/Co_3O_4(3D) and Pd/Co_3O_4(3DL). The XPS spectra clearly indicated that the Pd was in the oxidized state ($BE_{(Pd5/2)}$ higher than 335.6 eV) on both catalysts [29]. Fig. 7B shows the Co 2p XPS spectra of Co_3O_4(3D), Pd/Co_3O_4(3D) and Pd/Co_3O_4(3DL). The XPS spectra clearly indicate that there was a similar asymmetrical signal for each catalyst. The Co 2p XPS (Fig. 7B) suggests that the two methods had no observable effect on the valence state of cobalt oxide.

3.2.6. XAFS

XAFS measurements were conducted to study the detailed structure of samples. The XAFS of the Pd K-edge, including XANES and EXAFS, was measured using Pd foil and PdO as reference samples [30,31]. As shown in Fig. 8A, both the pre-edge peaks and the post-edge regions of Pd–K XANES in Pd/Co_3O_4(3D) and Pd/Co_3O_4(3DL) samples were similar to those in PdO, indicating the presence of Pd species in the oxidized state on these samples. The first-order derivatives of Pd–K XANES in Fig. 8B also confirmed that point of view. Table 3 shows the curve-fitted data of the filtered k3-weighted EXAFS oscillations of the Pd–K edge in Pd-containing samples and reference samples Fourier transformed into R space. For Pd/Co_3O_4(3D) and Pd/Co_3O_4(3DL) samples, Pd–O and Pd–O–Pd coordination shells were clearly observed,

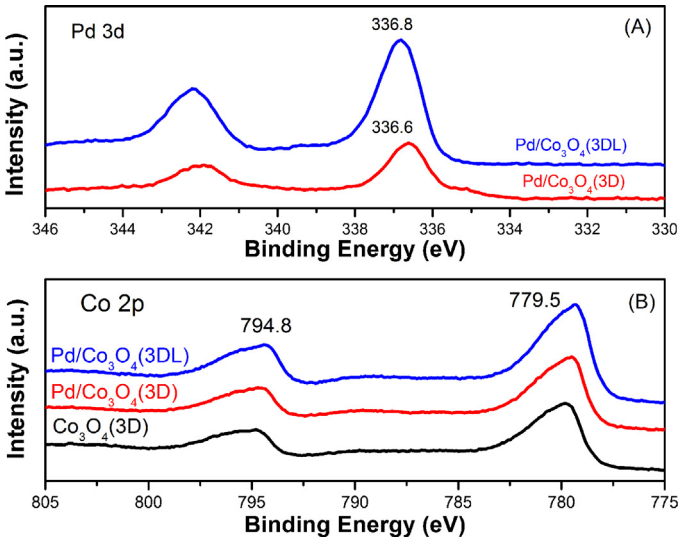

Fig. 7. (A and B) Pd 3d and Co 2p XPS spectra of the Pd based catalysts.

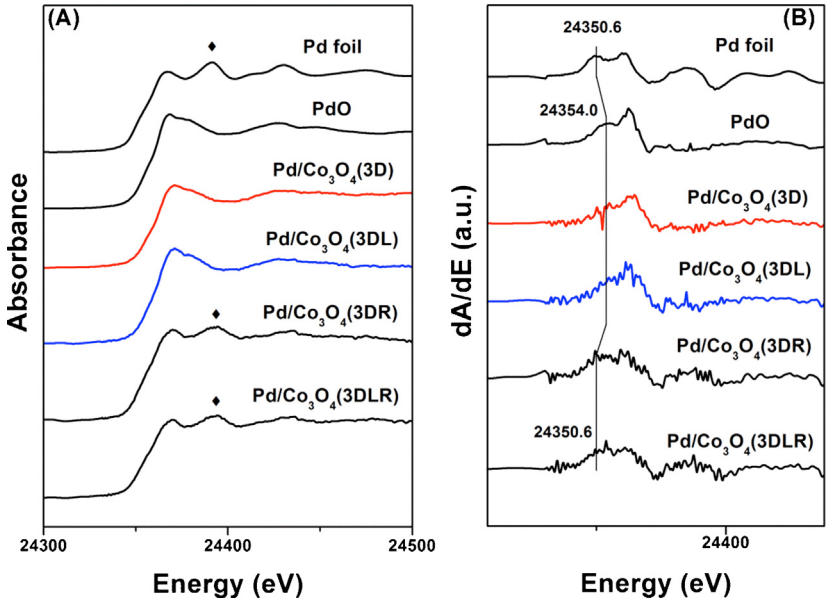

Fig. 8. (A) Normalized XANES and (B) first-order derivatives of XANES of the Pd K-edge in Pd-containing samples and reference samples.

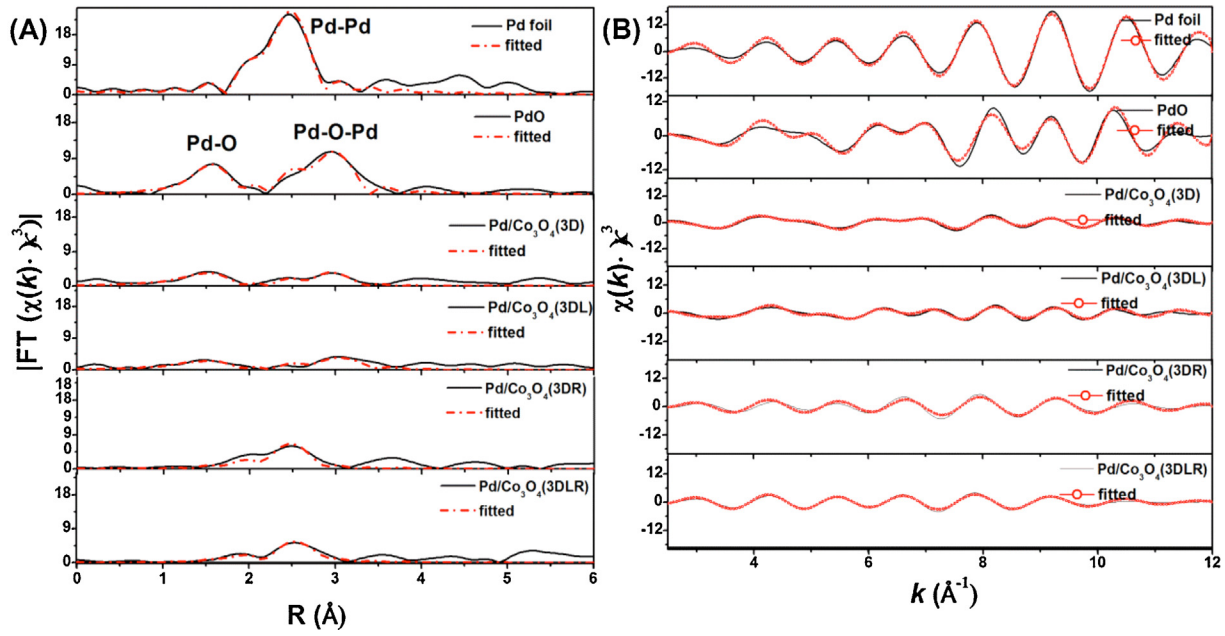

Fig. 9. EXAFS spectra of Pd K-edge in Pd-containing samples and reference samples: (A) Fourier transforms of filtered $k^3 \cdot \chi(k)$ into R space, where the dashed lines correspond to the curve fitting results; (B) filtered $k^3 \cdot \chi(k)$ in the k range of 2.5–12.0 Å^{-1}, where the dotted lines correspond to the curve fitting results.

yet no coordination shell attributed to Pd–O–Co was detected (Fig. 9). It is interesting to note that the coordination numbers of Pd–O–Pd shells (in Table 3) decreased in the following sequence: $Pd/Co_3O_4(3DL) > Pd/Co_3O_4(3D)$. In order to study the dispersion of Pd species, $Pd/Co_3O_4(3D)$ and $Pd/Co_3O_4(3DL)$ samples pre-reduced by H_2 (174 °C and 165 °C respectively) were also measured by XAFS. Both Pd–K EXAFS and Pd–K XANES results of the H_2-reduced $Pd/Co_3O_4(3DR)$ and $Pd/Co_3O_4(3DLR)$ suggest that Pd species were in the Pd^0 metallic phase after H_2 pre-treatment. Furthermore, the coordination number (6.6) of the Pd–Pd shell in $Pd/Co_3O_4(3DR)$ was much lower than that (8.8) of $Pd/Co_3O_4(3DLR)$ (shown in Table 3). We calculated the Pd metal particle sizes in $Pd/Co_3O_4(3DR)$ and $Pd/Co_3O_4(3DLR)$ according to the well-established relationship between noble metal particle size and metal–metal coordination number [32]. The calculated result showed that the Pd particle sizes in $Pd/Co_3O_4(3DR)$ and $Pd/Co_3O_4(3DLR)$ were 4.8 nm and 8.2 nm, respectively, indicating that the Pd species were more dispersed on $Pd/Co_3O_4(3D)$ than on $Pd/Co_3O_4(3DL)$.

In the Co–K edge XAFS study, $Co_3O_4(3D)$, $Pd/Co_3O_4(3D)$ and $Pd/Co_3O_4(3DL)$ samples both show Co–O, Co–O–Co_1 and Co–O–Co_2 peaks (in Fig. 11) with no significant differences in coordination numbers and bond lengths (in Table 4). The above-mentioned EXAFS results are also in good agreement with the XANES results in Fig. 10, reconfirming that the activity change in the o-xylene oxidation reaction was not correlated to the Co species.

3.3. Discussion

Fig. 1 and the specific activities data (Table 2) show that $Pd/Co_3O_4(3D)$ exhibited much better activity than $Pd/Co_3O_4(3DL)$, suggesting the Pd loading methods have an important influence on activity. First, the Pd loading method demonstrated an obvious effect on the mesostructures of catalysts. According to the XRD and BET results, we can see that $Pd/Co_3O_4(3D)$ had a much more ordered mesostructure than $Pd/Co_3O_4(3DL)$. When Pd was loaded using the in situ nanocasting method, the $Pd/Co_3O_4(3D)$ showed small angle peaks, surface area and pore size distribution similar

Table 4
Curve-fitting results of Co K-edge EXAFS in Co-containing samples and reference samples.

Sample	Shell	CN[a]	R[b] (Å)	σ^2 [c] (10^{-3} Å^2)	R factor (%)
Co foil	Co–Co	10.1	2.49	6.6	0.1
CoO	Co–O	3.6	2.11	5.8	0.8
	Co–O–Co	8.8	3.00	7.1	
Co_3O_4	Co–O	2.2	1.93	0.7	2.3
	Co–O–Co_1	1.9	2.85	2.1	
	Co–O–Co_2	4.6	3.35	5.9	
Co_3O_4(3D)	Co–O	3.3	1.92	2.2	2.5
	Co–O–Co_1	2.5	2.84	2.2	
	Co–O–Co_2	7.3	3.34	8.3	
Pd/Co_3O_4(3D)	Co–O	3.2	1.92	2.1	2.0
	Co–O–Co_1	2.8	2.85	3.0	
	Co–O–Co_2	6.1	3.35	6.9	
Pd/Co_3O_4(3DL)	Co–O	3.3	1.92	2.1	2.6
	Co–O–Co_1	2.7	2.85	3.0	
	Co–O–Co_2	6.0	3.35	7.2	

[a] CN: coordination number.
[b] R: bond distance.
[c] σ: Debye–Waller factor.

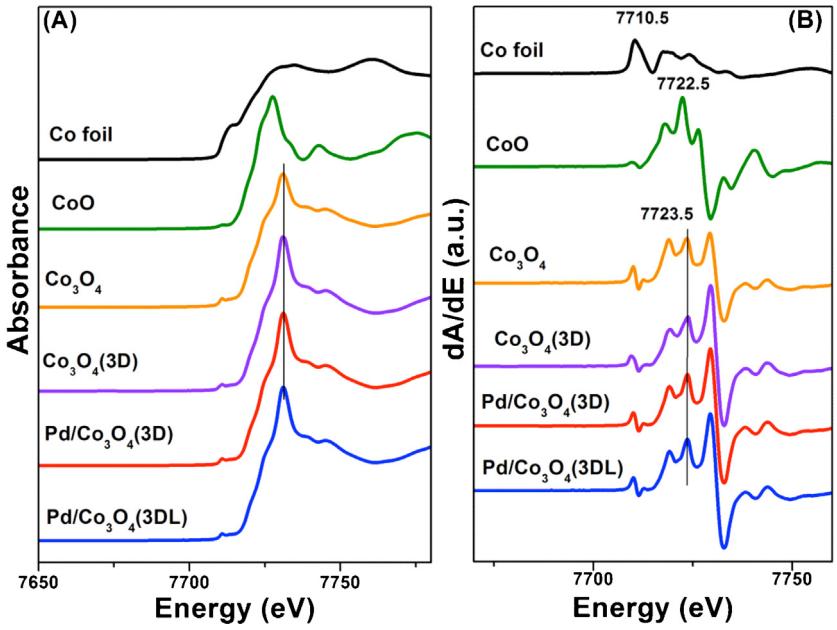

Fig. 10. (A) Normalized XANES and (B) first-order derivatives of XANES of Co K-edge in Co-containing samples and reference samples.

to Co_3O_4(3D), showing that the mesostructure of Co_3O_4(3D) was not much affected. In contrast, when Pd was loaded using the post-impregnation method, the Pd/Co_3O_4(3DL) exhibited a much lower XRD peak intensity, lower surface area and wider distribution of pore size than that of Co_3O_4(3D), indicating its less ordered mesostructure, which can be observed in the TEM images (Fig. 5C)). During the in situ nanocasting process, the cobalt and Pd precursors were simultaneously dispersed and transferred into the meso-channels of the silica template (KIT-6), and then grew into cobalt oxide and PdO by self-assembly in the meso-channels of the template, leading to metal oxide nanocrystals with uniform size and then aggregating to an ordered mesostructure during the following pyrolysis [33]. When the Pd precursor was post-impregnated into Co_3O_4(3D), the mesostructure of Co_3O_4(3D) could be partially destroyed (in Fig. 5C) during the impregnation and re-calcination process without the restriction imposed by the template.

The preparation method also had an observable effect on the dispersion of PdO, the active material on the supports. XPS results (Fig. 7A) showed that the Pd 3d peak intensity in Pd/Co_3O_4(3D) was much lower than that in Pd/Co_3O_4(3DL), demonstrating that the PdO species were mainly dispersed on the Co_3O_4(3D) surface when loaded by post-impregnation, but mainly embedded in the Co_3O_4(3D) mesostructure skeleton when loaded by in situ nanocasting. Although the XRD results (Fig. 3) showed that PdO species were well dispersed on both Pd/Co_3O_4(3D) and Pd/Co_3O_4(3DL) catalysts, TPR results demonstrated that the PdO

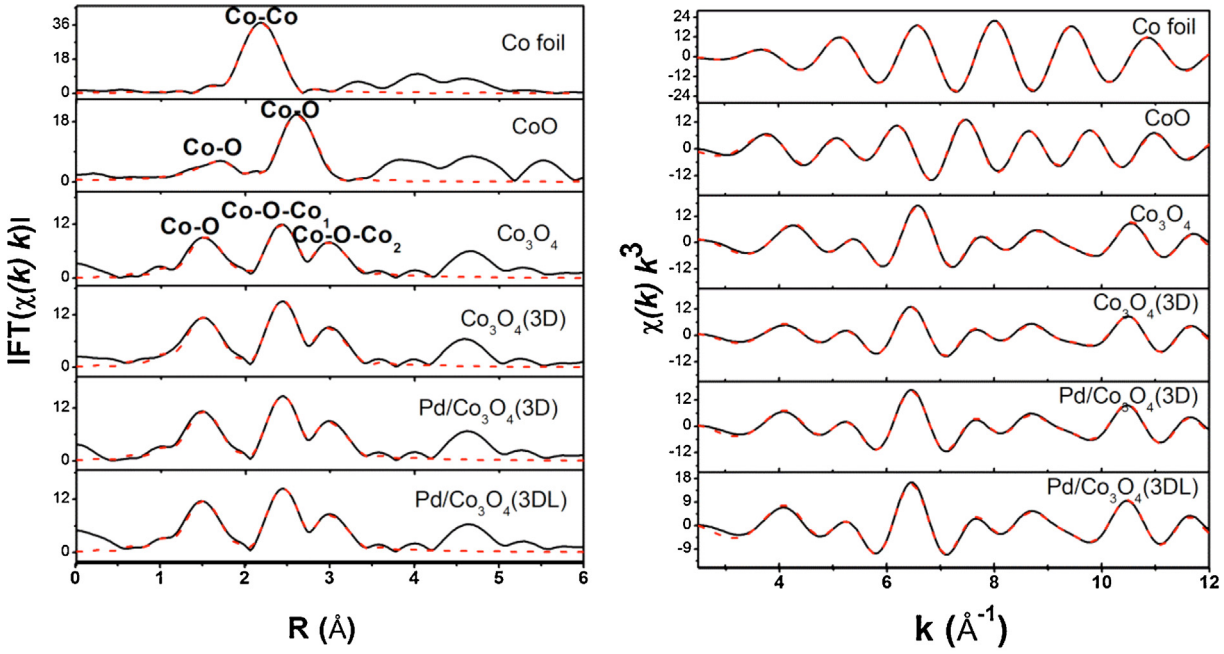

Fig. 11. EXAFS spectra of Co K-edge in Co-containing samples: (A) Fourier transforms of filtered $k^3 \cdot \chi(k)$ into R space, where the dashed lines correspond to the curve fitting results; (B) filtered $k^3 \cdot \chi(k)$ in the k range of 2.5–13.0 Å^{-1}, where the dotted lines correspond to the curve fitting results.

species were more uniformly dispersed on the former than on Pd/Co_3O_4(3DL), because Pd/Co_3O_4(3D) presented a much sharper PdO reduction peak than Pd/Co_3O_4(3DL). The TPR results also demonstrated that the PdO reduction temperature of Pd/Co_3O_4(3D) was higher than that of Pd/Co_3O_4(3DL), indicating a much stronger interaction of the PdO component with Co_3O_4 in the former catalyst. In addition, the Pd particle sizes calculated based on EXAFS results (Fig. 9 and Table 3) indicate that the Pd particle size (4.8 nm) on Pd/Co_3O_4(3DR) was much smaller than that (8.2 nm) on Pd/Co_3O_4(3DLR), further confirming that the in situ nanocasting synthesis method was beneficial to the formation of more dispersed oxidized Pd species with much smaller particle size.

The well-defined three-dimensional ordered mesoporous structure could facilitate the adsorption and diffusion of o-xylene molecules, and the highly dispersed PdO species could contribute to the easy activation of the oxygen and o-xylene during the catalytic oxidation process. Therefore, the Pd/Co_3O_4(3D) synthesized by the in situ nanocasting method demonstrated much better activity for o-xylene oxidation than Pd/Co_3O_4(3DL) prepared with the post-impregnation method.

4. Conclusions

Co_3O_4(3D)-supported Pd catalysts were prepared by in situ nanocasting and post-impregnation methods, respectively. Pd/Co_3O_4(3D) showed much better activity than Pd/Co_3O_4(3DL) for the catalytic oxidation of o-xylene, achieving 100% o-xylene conversion at around 200 °C. The characterization results revealed that Pd/Co_3O_4(3D) synthesized by the in situ nanocasting method had a more ordered mesostructure and also more well-dispersed PdO species than Pd/Co_3O_4(3DL) prepared by the post-impregnation method. Therefore, the excellent catalytic performance of Pd/Co_3O_4(3D) is attributed to its uniform mesostructure and the highly dispersed PdO with small particle size on Co_3O_4(3D). This in situ nanocasting approach may be applicable to the synthesis of other metals supported on mesostructured materials with ordered meso-structure and dispersed metal species.

Acknowledgments

This work was financially supported by the National High Technology Research and Development Program of China (2010AA64905 and 2012AA062702) and the National Natural Science Foundation of China (21077117). The authors sincerely thank the staff from the BL14W1 beam line, Shanghai Synchrotron Radiation Facility (SSRF) for their generous help in XAFS experiments.

Appendix A. Supplementary data

Supplementary data associated with this article can be found, in the online version, at http://dx.doi.org/10.1016/j.apcatb.2013.05.003.

References

[1] A. Jones, Atmos. Environ. 33 (1999) 4535–4564.
[2] F.I. Khan, Kr.A. Ghoshal, J. Loss Prevent. Proc. 13 (2000) 527–545.
[3] P. Gélin, M. Primet, Appl. Catal. B: Environ. 39 (2002) 1–37.
[4] J.R. González-Velasco, A. Aranzabal, J.I. Gutiérrez-Ortiz, R. López-Fonseca, M.A. Gutiérrez-Ortiz, Appl. Catal. B: Environ. 19 (1998) 189–197.
[5] L.F. Liotta, Appl. Catal. B: Environ. 100 (2010) 403–412.
[6] S. Huang, C. Zhang, H. He, Catal. Today 139 (2008) 15–23.
[7] R. Burch, P.K. Loader, F.J. Urbano, Catal. Today 27 (1996) 243–248.
[8] S.-K. Ihm, Y.-D. Jun, D.-C. Kim, K.-E. Jeong, Catal. Today 93–95 (2004) 149–154.
[9] P. Dégé, L. Pinard, P. Magnoux, M. Guisnet, Appl. Catal. B: Environ. 27 (2000) 17–26.
[10] Y. Yazawa, H. Yoshida, N. Takagi, S.-i. Komai, A. Satsuma, T. Hattori, Appl. Catal. B: Environ. 19 (1998) 261–266.
[11] K. Okumura, T. Kobayashi, H. Tanaka, M. Niwa, Appl. Catal. B: Environ. 44 (2003) 325–331.
[12] H.L. Tidahy, S. Siffert, J.F. Lamonier, R. Cousin, E.A. Zhilinskaya, A. Aboukais, B.L. Su, X. Canet, G. De Weireld, A. Frere, J.M. Giraudon, G. Leclercq, Appl. Catal. B: Environ. 70 (2007) 377–383.
[13] G. Centi, J. Mol. Catal. A: Chem. 173 (2001) 287–312.
[14] W.B. Yue, W.Z. Zhou, Prog. Nat. Sci. 18 (2008) 1329–1338.
[15] P. Yang, D. Zhao, D.I. Margolese, B.F. Chmelka, G.D. Stucky, Nature 396 (1998) 152–155.
[16] B.Z. Tian, X.Y. Liu, L.A. Solovyov, Z. Liu, H.F. Yang, Z.D. Zhang, S.H. Xie, F.Q. Zhang, B. Tu, C.Z. Yu, O. Terasaki, D.Y. Zhao, J. Am. Chem. Soc. 126 (2004) 865–875.
[17] T. Tsoncheva, L. Ivanova, J. Rosenholm, M. Linden, Appl. Catal. B: Environ. 89 (2009) 365–374.
[18] A. Rumplecker, F. Kleitz, E.L. Salabas, F. Schuth, Chem. Mater. 19 (2007) 485–496.
[19] H. Tüysüz, M. Comotti, F. Schüth, Chem. Commun. (2008) 4022–4024.
[20] Y. Xia, H. Dai, H. Jiang, L. Zhang, Catal. Commun. 11 (2010) 1171–1175.
[21] J. Deng, L. Zhang, H. Dai, Y. Xia, H. Jiang, H. Zhang, H. He, J. Phys. Chem. C 114 (2010) 2694–2700.
[22] F. Kleitz, S. Hei Choi, R. Ryoo, Chem. Commun. (2003) 2136.
[23] Y. Yu, T. Takei, H. Ohashi, H. He, X. Zhang, M. Haruta, J. Catal. 267 (2009) 121–128.
[24] J.J.W. Cook, D.E. Sayers, J. Appl. Phys. 52 (1981) 5024–5031.
[25] A.L. Ankudinov, B. Ravel, J.J. Rehr, S.D. Conradson, Phys. Rev. B 58 (1998) 7565–7576.
[26] M. Newville, J. Synchrotron Radiat. 8 (8) (2001) 322–324.
[27] M. Kruk, M. Jaroniec, Chem. Mater. 13 (2001) 3169–3183.
[28] X. Xie, Y. Li, Z.-Q. Liu, M. Haruta, W. Shen, Nature 458 (2009) 746–749.
[29] G.E. Muilenberg, Handbook of X-ray photoelectron spectroscopy, Perkin- Elmer Corporation, Eden Prairie, Minnesota, 1979, pp. 110.
[30] K. Okumura, K. Nota, K. Yoshida, M. Niwa, J. Catal. 231 (2005) 245–253.
[31] K. Shimizu, S. Koizumi, T. Hatamachi, H. Yoshida, S. Komai, T. Kodama, Y. Kitayama, J. Catal. 228 (2004) 141–151.
[32] B.J. Kip, F.B.M. Duivenvoorden, D.C. Koningsberger, R. Prins, J. Catal. 105 (1987) 26–38.
[33] Y. Wan, H.F. Yang, D.Y. Zhao, Acc. Chem. Res. 39 (2006) 423–432.